Scientific Research Publishing

Energy and Power Engineering, 2022, 14, 248-273
https://www.scirp.org/journal/epe
ISSN Online: 1947-3818
ISSN Print: 1949-243X

Impact of Separator Thickness on Temperature Distribution in Single Polymer Electrolyte Fuel Cell Based on 1D Heat Transfer

Akira Nishimura*, Daiki Mishima, Nozomu Kono, Kyohei Toyoda, Mohan Lal Kolhe

Mie University, Tsu, Japan
Email: *nisimura@mach.mie-u.ac.jp

How to cite this paper: Nishimura, A., Mishima, D., Kono, N., Toyoda, K. and Kolhe, M.L. (2022) Impact of Separator Thickness on Temperature Distribution in Single Polymer Electrolyte Fuel Cell Based on 1D Heat Transfer. *Energy and Power Engineering*, **14**, 248-273.
https://doi.org/10.4236/epe.2022.147014

Received: May 30, 2022
Accepted: July 24, 2022
Published: July 27, 2022

Abstract

It is known from the New Energy and Industry Technology Development Organization (NEDO) roam map Japan, 2017 that the polymer electrolyte fuel cell (PEFC) power generation system is required to operate at 100˚C for application of mobility usage from 2020 to 2025. This study aims to clarify the effect of separator thickness on the distribution of the temperature of reaction surface (T_{react}) at the initial temperature of cell (T_{ini}) with flow rate, relative humidity (RH) of supply gases as well as RH of air surrounding cell of PEFC. The distribution of T_{react} is estimated by means of the heat transfer model considering the H_2O vapor transfer proposed by the authors. The relationship between the standard deviation of T_{react}-T_{ini} and total voltage obtained in the experiment is also investigated. We can know the effect of the flow rate of supply gas as well as RH of air surrounding cell of PEFC on the distribution of T_{react}-T_{ini} is not significant. It is observed the wider distribution of T_{react}-T_{ini} provides the reduction in power generation performance irrespective of separator thickness. In the case of separator thickness of 1.0 mm, the standard deviation of T_{react}-T_{ini} has smaller distribution range and the total voltage shows a larger variation compared to the other cases.

Keywords

Polymer Electrolyte Fuel Cell, Heat Transfer Modeling, H_2O Vapor Transfer, Temperature Distribution, High Temperature

1. Introduction

Recently, it is thought that renewable energy is desirable as one solution to solve global warming and H_2 is considered to be one procedure to preserve and

transport renewable energy as well as battery since photovoltaic and wind power have time variability. Polymer electrolyte fuel cell (PEFC) which is one type of fuel cell (FC) is a popular application to use H_2 as a fuel that can generate power and heat. In Japan, New Energy and Industrial Technology Development (NEDO)'s road map Japan, 2017 [1] has declared that PEFC should be operated at around 100˚C for mobility application respectively, which targets the duration from the year 2020 to 2025. However, PEFC using polymer electrolyte membrane (PEM) e.g. Nafion is usually operated from 60˚C to 80˚C [2] [3] [4]. If we operate PEFC at a relatively higher temperature than usual, *i.e.* 100˚C, the following merits can be obtained: 1) promotion of electrochemical kinetics of both electrodes; 2) reduction in the cooling system for mobile application due to a larger temperature gap between the PEFC stack and coolant; 3) enhancement of endurance to CO which can be available on the low quality of reformed H_2, 4) H_2O management is simplified since we can consider a single phase of H_2O only, 5) waste heat can be utilized as an energy source [5] [6]. However, we need to consider the following problems if we operate the PEFC system at a higher temperature than usual: 1) degradation of PEM, 2) erosion of catalyst, 3) uneven distributions of gas flow, pressure, temperature, voltage and current. We should solve these problems in order to commercialize the PEFC system which operates at relatively high temperatures [5]. Additionally, the temperature distribution also provides the impact on 1) the phase change of H_2O, 2) the performance of PEM, and 3) fuel and oxidant flows in the gas diffusion layer (GDL) and the electrode at a higher temperature than usual. Consequently, it is necessary to understand the temperature distribution in a single PEFC to promote the power generation performance and extend the operational life span of the PEFC system.

High Temperature PEFC (HTPEFC) has been focused recently on temperature above 100˚C [7]-[14]. Most of them can be categorized into the R & D of new materials, which can work at a higher temperature, e.g. membrane and catalyst [7]-[14]. Focused on the research to understand the heat and mass transfer characteristics in HTPEFC, some numerical studies have reported that the temperature-driven H_2O transport in cathode GDL [15], optimization of electrode thickness to obtain higher performance without high cost [16], assessment of mass transport effect on the performance by 3D multi-physics modeling [17], optimization of GDL focusing the thickness of porosity by non-isothermal 3D model [18] and dynamic simulation for start-up process by non-isothermal 3D model [4]. Some numerical studies [19] [20] [21] have reported analysis on separators to optimize a gas channel considering the widths of top and bottom, e.g. cross-sectional area with a trapezium shape [19], the investigation of power generation performance, reactant and H_2O saturation distribution using oriented-type flow channels with porous-blocked baffles [20], and the impact of the ratio of channel width to rib width on the performance and mass distribution in the cell [21]. A few researchers [4] [22] [23] have reported numerical simulation on temperature distribution in a single PEFC which is operated at a higher temperature than usual. However, only a few papers [4] [22] have investigated the tempera-

ture distribution on the interface between PEM and electrode at the cathode, which is defined as the reaction surface in this study, excluding the research conducted by the authors [24] [25] [26] [27]. The previous studies [24] [25] [26] [27] have confirmed the thickness effect of not only PEM but also GDL on the distribution of temperature at reaction surface (T_{react}) in a single PEFC at a higher temperature, *i.e.* 90˚C or 100˚C by the heat transfer model using the experimental temperature distribution data gotten by means of thermograph. However, the effect of separator thickness including saddle thickness and channel height on the distribution of T_{react} has not been investigated yet. The separator thickness influences the weight, volume and cost of PEFC stack since the commercial PEFC stack is composed of several hundreds of cells. Consequently, it is necessary to clarify the effect of separator thickness on the distribution of T_{react} in order to commercialize the PEFC stack operated at higher temperature than usual.

This study aims to clarify the thickness effect of separator on the distribution of T_{react} in single PEFC changing flow rates, relative humidity (RH) of supply gases at initial operation temperature (T_{ini}) of 100˚C. The effect of RH of air surrounding the single PEFC on the distribution of T_{react} is investigated. Using thinner PEM and thinner GDL at the same time is adopted for this analysis. The previous studies conducted by the authors [24] [25] [26] [27] have clarified using thinner PEM and thinner GDL at the same time is effective in order to obtain higher power generation performance of PEFC operated at higher temperature, *i.e.* 90˚C and 100˚C. The authors have measured the temperature distributions on separator's back of a cell of PEFC by means of thermograph, which is applied to the heat transfer model developed by the authors [28] [29]. Since this procedure can measure the temperature distribution with no disturbance of the heat and mass transfer phenomena and power generation characteristics because of sensor installation, it can be claimed that the temperature distribution during the power generation can be measured accurately. Using the measured data, the previous studies [27] [30] [31] have challenged to develop an empirical model in order to predict the distributions of T_{react}. Though the authors have reviewed the literature, it is confirmed there is no previous study to estimate the distribution of T_{react} using the temperature data at separator's back. The heat transfer model proposed by this study can predict the distributions of T_{react} using the measured separator's back, and it is favorable to analyze through a model. The distribution of T_{react} can be estimated easily with no difficult and complex temperature measurement by the proposed heat transfer model. Additionally, this study also develops the model considering the H_2O vapor transfer through the components of cell as well as heat transfer. Since the H_2O vapor transfer through the cell components has not been considered in the past model [24] [25] [26] [27], this is a brand-new procedure to make a prediction on the distribution of T_{react}.

In the studies carried out by the authors [24] [25] [26] [27], a 1D multi-plate heat transfer model which uses the temperature data of separator's back measured by means of the thermograph with power generation has been developed. Single PEFC is composed of PEM, catalyst layer, MPL, GDL and separator. The

model proposed by the authors [24] [25] [26] [27] has assumed that all heat flows through multi-plates of these cell components. This study calculates the temperature at the interface between PEM and catalyst later on the cathode, *i.e.* T_{react} by the heat transfer model [24] [25] [26] [27]. This is a brand-new procedure to clarify the heat transfer characteristics in a single PEFC using the experimental data obtained by means of the thermograph and the proposed model.

2. Numerical Analysis Procedure

2.1. 1D Multi-Plate Heat Transfer Model

Figure 1 shows the multi-plate single cell of the PEFC module proposed by this study. In this module, the separator's back is the opposite side of the surface contacting with GDL. The separator's back surface temperatures $T_{surf,\,c}$ and $T_{surf,\,a}$ are measured by the thermograph. This study assumes the heat transfer across the module is to be in 1D direction only. In this module, this study divides the cell into a channel and a rib part, and the upper and lower parts indicate rib part and channel part, respectively. This study assumes the heat transfer is to be in the through-plane direction for both parts.

This study assumes the heat generated on the reaction surface is transferred to cathode and anode sides separately. Though the gas which flows through the gas channel from the inlet to the outlet of the cell transports a heat, the total amount of heat taken is below 1% of the calculated reaction heat of about 20 W [32]. Consequently, this study considered that the heat transported by the gas flow can be ignored in this model. In addition, the mass flow rate of gas flowing through the gas channel is very little which ranges from 10^{-8} to 10^{-6} kg/s. Therefore,

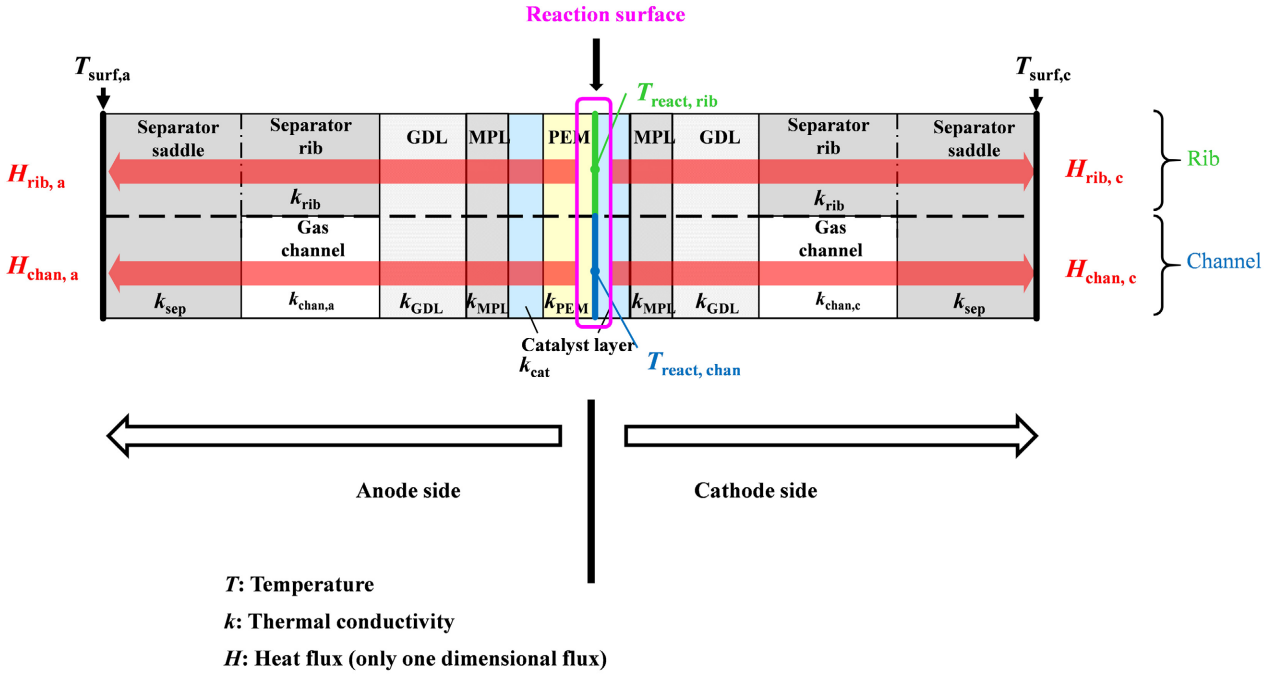

Figure 1. Schematic drawing of 1D multi-plate heat transfer module.

this study can assume the thermal conduction of gas in the gas channel only since the gas flow is thought to be static. The other studies on the numerical simulation conducted by 3D model considering the phase change of H_2O [27] [33] have reported that the temperature difference between T_{react} under the rib and that under the channel is small, which is about within 1˚C at the temperature of 70˚C - 80˚C. Consequently, it can be thought the effect of the heat pipe that supports the heat removal under the channel is small.

2.2. Heat Generation Rate by Reaction in the Model Proposed by This Study

The heat generation rate H_{react} produced by reaction can be calculated as follows [24] [25] [26] [27]:

$$H_{react} = E_i - W_E \tag{1}$$

where E_i indicates the ideal (total) energy generation rate from the H_2O formation by H_2 and O_2 which is estimated by the higher heating value (q_{HHV}). W_E indicates the electric work produced by PEFC. E_i and W_E are defined as following [24] [25] [26] [27]:

$$E_i = m_{H2} \times q_{HHV} \tag{2}$$

$$W_E = I \times V \tag{3}$$

where I indicates the total current gotten by the power generation experiment. The power generation data obtained at the load current of 20 A (=0.80 A/cm^2) which are applied for proposed heat transfer model. V indicates the total voltage and obtained by the power generation experiment. m_{H2} indicates the molar flow rate of supplied H_2, which is the same as the ideal reaction consumption rate of H_2 needed for the power generation at 20 A, *i.e.*, the stoichiometric ratio (s.r.) of 1.0, where s.r. means the ratio of the feed amount of H_2 and O_2 to that needed to generate a current of 20 A. The flow rate of supply gas (H_2) at s.r. of 1.0 can be defined as following [24] [25] [26] [27]:

$$m_{H2} = I/nF \tag{4}$$

where m_{H2} indicates the molar flow rate of supplied H_2 (mol/s), n indicates the valence of ion (=2 in case of H_2), F indicates the Faraday constant (=96,500 C/mol). m_{O2} indicates the molar flow rate of supplied O_2 (mol/s) and it can be estimated as following [24] [25] [26] [27]:

$$H_2 + 1/2\,O_2 = H_2O \tag{5}$$

The s.r. of supply gases is confirmed actually by means of the mass flow controller which is set up at the inlet of the single cell. Additionally, the mass flow meter is set up at the outlet of the cell in the power generation experiment [28]. The consumption rates of supplied H_2 and O_2 are s.r. of 1.0 respectively, which is confirmed from the power generation experiment.

2.3. Heat-Balance Formulas to Calculate Reaction Surface Temperature

In the proposed model, the transferred heats can be expressed as Equations

(6)-(10), which are mentioned in the reference [34].

$$H_{\text{rib,c}} = K_{\text{rib,c}} A\left(T_{\text{react,rib}} - T_{\text{surf,c}}\right)/2 \tag{6}$$

$$H_{\text{chan,c}} = K_{\text{chan,c}} A\left(T_{\text{react,chan}} - T_{\text{suf,c}}\right)/2 \tag{7}$$

$$H_{\text{rib,a}} = K_{\text{rib,a}} A\left(T_{\text{react,rib}} - T_{\text{surf,a}}\right)/2 \tag{8}$$

$$H_{\text{chan,a}} = K_{\text{chan,a}} A\left(T_{\text{react,chan}} - T_{\text{surf,a}}\right)/2 \tag{9}$$

$$H_{\text{react}} = H_{\text{rib,c}} + H_{\text{chan,c}} + H_{\text{rib,a}} + H_{\text{chan,a}} \tag{10}$$

where $H_{\text{rib,c}}$ means the heat flux through cathode side under rib (W), $K_{\text{rib,c}}$ means the overall heat transfer coefficient through cathode side under rib (W/(m^2·K)), A means the heat transfer area which equals to the active area of MEA, *i.e.*, power generation area (=0.0025 m^2), $T_{\text{react,rib}}$ means the temperature of reaction surface under rib (K or ˚C), $T_{\text{surf,c}}$ means the separator's back surface temperature at cathode (K or ˚C), $H_{\text{chan,c}}$ means the heat flux through cathode side under channel (W), $K_{\text{chan,c}}$ means the overall heat transfer coefficient through cathode side under channel (W/(m^2·K)), $T_{\text{react,chan}}$ means the temperature of reaction surface under channel (K or ˚C), $H_{\text{rib,a}}$ means the heat flux through anode side under rib (W), $K_{\text{rib,a}}$ means the overall heat transfer coefficient through anode side under rib (W/(m^2·K)), $T_{\text{surf,a}}$ means the separator's back temperature at anode (K or ˚C), $H_{\text{chan,a}}$ means the heat flux through anode side under channel (W), $K_{\text{chan,a}}$ means the overall heat transfer coefficient through anode side under channel (W/(m^2·K)). $K_{\text{rib,c}}$, $K_{\text{chan,c}}$, $K_{\text{rib,a}}$ and $K_{\text{chan,a}}$ can be defined as following:

$$1/K_{\text{rib,c}} = d_{\text{cat}}/k_{\text{cat}} + d_{\text{MPL}}/k_{\text{MPL}} + d_{\text{GDL}}/k_{\text{GDL}} + d_{\text{rib}}/k_{\text{rib}} + d_{\text{sep}}/k_{\text{sep}} \tag{11}$$

$$1/K_{\text{chan,c}} = d_{\text{cat}}/k_{\text{cat}} + d_{\text{MPL}}/k_{\text{MPL}} + d_{\text{GDL}}/k_{\text{GDL}} + d_{\text{chan}}/k_{\text{chan,c}} + d_{\text{sep}}/k_{\text{sep}} \tag{12}$$

$$1/K_{\text{rib,a}} = d_{\text{PEM}}/k_{\text{PEM}} + d_{\text{cat}}/k_{\text{cat}} + d_{\text{MPL}}/k_{\text{MPL}} + d_{\text{GDL}}/k_{\text{GDL}} + d_{\text{rib}}/k_{\text{rib}} + d_{\text{sep}}/k_{\text{sep}} \tag{13}$$

$$1/K_{\text{chan,a}} = d_{\text{PEM}}/k_{\text{PEM}} + d_{\text{cat}}/k_{\text{cat}} + d_{\text{MPL}}/k_{\text{MPL}} + d_{\text{GDL}}/k_{\text{GDL}} + d_{\text{chan}}/k_{\text{chan,a}} + d_{\text{sep}}/k_{\text{sep}} \tag{14}$$

where d_{cat} means the thickness of the catalyst layer (m), k_{cat} means the thermal conductivity of the catalyst layer (W/(m·K)), d_{MPL} means the thickness of MPL (m), k_{MPL} means the thermal conductivity of MPL (W/(m·K), d_{GDL} means the thickness of GDL (m), k_{GDL} means the thermal conductivity of GDL (W/(m·K)), d_{rib} means the thickness of the separator rib (m), k_{rib} means the thermal conductivity of the separator rib (W/(m·K)), d_{sep} means thickness of the separator except for rib (m), k_{sep} means the thermal conductivity of the separator except for rib (W/(m·K)), d_{chan} means thickness of the channel of separator (m), k_{chan} means the thermal conductivity of the mixed gas in the channel of separator (W/(m·K)), d_{PEM} means the thickness of PEM (m), k_{PEM} means the thermal conductivity of PEM (W/(m·K)).

Table 1 shows the specification of cell components applied for the proposed model. Nafion NRE-211 (produced by Du Pont Corp.) with a thickness of 25 micron

Table 1. Specification on components of single PEFC according to the manufacture's catalog and previous studies [24]-[29].

Components	Dimension	Characteristics	Porosity [-]	Effective thermal conductivity [W/(m·K)]
Polymer electrolyte membrane (PEM)	50.0 mm × 50.0 mm × 0.025 mm	Nafion NRE-211 (produced by Du Pont Corp.)	0.28	0.195
Catalyst layer	50.0 mm × 50.0 mm × 0.01 mm	Pt/C (20 wt% loading)	0.78	0.27
Micro porous layer (MPL)	50.0 mm × 50.0 mm × 0.003 mm	Mixture of carbon black and PTFE	0.60	1.0
Gas diffusion layer (GDL)	50.0 mm × 50.0 mm × 0.11 mm	TGP-H-030 (produced by Toray Corp.)	0.78	1.7
Separator	75.4 mm × 75.4 mm × 2.0 mm (saddle thickness = 1.0 mm, channel height = 1.0 mm) or 1.5 mm (saddle thickness = 0.5 mm, channel height = 1.0 mm) or 1.0 mm (saddle thickness = 0.5 mm, channel height = 0.5 mm)	Carbon graphite, separator	0.15	2

and TGP-H-030 (produced by Toray Corp.) with a thickness of 110 micron are adopted in this study. The proposed model is composed of PEM, catalyst layer, MPL, GDL and separator. Table 1 lists some values of components, which are the same as the previous studies [24] [25] [26] [27].

Table 1 also lists the effective thermal conductivities of porous media k [28] [29] [35], which are the same as the values of cell components used in the experiment carried out by the authors [28] [29]. According to Table 2, the effective thermal conductivities are listed under the condition that the pores of cell components are fulfilled with air at room temperature. The corrected effective thermal conductivities are estimated under the condition that the pores of cell components are fulfilled with H_2 or O_2 at 100˚C, which represents T_{ini} in this study. As to the power generation experiment whose data were applied for the heat transfer model proposed by this study [29], the single PEFC was pre-pared by electric heater at T_{ini} for the power generation experiment to measure the temperature by means of thermograph. Additionally, this study controls the temperature of supply gas by electric heater at T_{ini}. Thermal conductivities of each supply gases are referred from "The Japan Society of Mechanical Engineers" [36] in this calculation.

Additionally, this study considers the H_2O vapor transfer from the catalyst layer at the cathode. The H_2O produced by electro-chemical reaction transfers to the outside of the single PEFC by the gas diffusion. Figure 2 shows 1D multi-plate H_2O vapor transfer model. e means porosity (-).

This study estimates the H_2O vapor concentration in catalyst layer at the cathode by adding the H_2O produced by electro-chemical reaction. It is mixed with the H_2O in supplied gas in the cell, which indicates the RH of supply gas. We

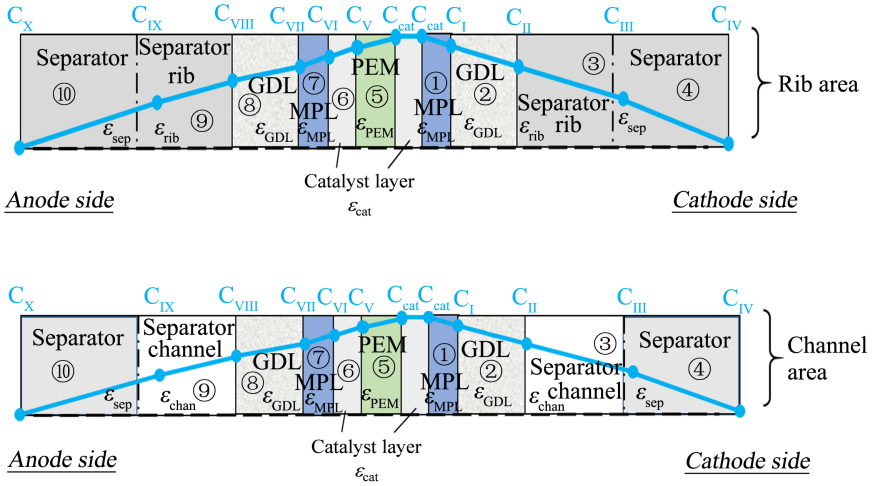

Figure 2. 1D multi-plate H_2O vapor transfer module.

Table 2. Diffusivity of H_2O vapor which is applied for considering the H_2O vapor transfer in the cell [37] [38].

H_2O-H_2 [m^2/s]	9.27×10^{-5}
H_2O-O_2 [m^2/s]	3.57×10^{-5}
PEM (40% RH) [m^2/s]	3.958×10^{-7}
PEM (80% RH) [m^2/s]	1.166×10^{-6}

divide the cell into twenty segments as explained later. This study divides the amount of H_2O produced by electro-chemical reaction into twenty segments equally, and this study assumes to add it with gas flows through segments. Due to consumption of H_2 and O_2 by electro-chemical reaction in anode side and cathode side, respectively, the concentration of H_2 and O_2 in catalyst layer at anode and cathode, respectively, decreases from the inlet to the outlet through segments gradually, which was confirmed by the study on numerical simulation with 3D model [39]. In addition, the in-plane molar concentration distribution of H_2O on the interface between PEM and catalyst layer at cathode increases gradually along with the gas flow through the gas channel [39]. Therefore, this study has divided the amount of produced H_2O into twenty segments equally in order to confirm the regularity of phenomena. This study estimates the H_2O vapor concentration in catalyst layer at cathode by considering the change in H_2O vapor and O_2. It is a meaningful to understand the diffusivity of H_2O vapor in each component of single cell. **Table 2** shows diffusivity of H_2O vapors applied in this study.

This study assumes a binary diffusion of H_2O, and H_2 or O_2 is conducted in each component excluding PEM. Regarding PEM, the H_2O vapor is transported via electro-osmotic drag with H^+, depending on H_2O content in PEM [36]. The relation between RH of supply gas and diffusivity of H_2O vapor in PEM is followed from the reference [37]. The H_2O vapor transfer can be estimated by Equations (15)-(26).

$$w_{\mathrm{I}} = -D_{\mathrm{H_2O\text{-}O_2}}\left(C_{\mathrm{I}} - C_{\mathrm{cat}}\right)/d_{\mathrm{MPL}}e_{\mathrm{MPL}} \tag{15}$$

$$w_{\mathrm{II}} = -D_{\mathrm{H_2O\text{-}O_2}}\left(C_{\mathrm{II}} - C_{\mathrm{I}}\right)/d_{\mathrm{GDL}}e_{\mathrm{GDL}} \tag{16}$$

$$w_{\mathrm{III}} = -D_{\mathrm{H_2O\text{-}O_2}}\left(C_{\mathrm{III}} - C_{\mathrm{II}}\right)/d_{\mathrm{Rib}}e_{\mathrm{Rib}} \tag{17}$$

$$w_{\mathrm{IV}} = -D_{\mathrm{H_2O\text{-}O_2}}\left(C_{\mathrm{IV}} - C_{\mathrm{III}}\right)/d_{\mathrm{sep}}e_{\mathrm{sep}} \tag{18}$$

$$w_{\mathrm{V}} = -D_{\mathrm{PEM}}\left(C_{\mathrm{V}} - C_{\mathrm{cat}}\right)/d_{\mathrm{PEM}}e_{\mathrm{PEM}} \tag{19}$$

$$w_{\mathrm{VI}} = -D_{\mathrm{H_2O\text{-}H_2}}\left(C_{\mathrm{VI}} - C_{\mathrm{V}}\right)/d_{\mathrm{cat}}e_{\mathrm{cat}} \tag{20}$$

$$w_{\mathrm{VII}} = -D_{\mathrm{H_2O\text{-}H_2}}\left(C_{\mathrm{VII}} - C_{\mathrm{VI}}\right)/d_{\mathrm{MPL}}e_{\mathrm{MPL}} \tag{21}$$

$$w_{\mathrm{VIII}} = -D_{\mathrm{H_2O\text{-}H_2}}\left(C_{\mathrm{VIII}} - C_{\mathrm{VII}}\right)/d_{\mathrm{GDL}}e_{\mathrm{GDL}} \tag{22}$$

$$w_{\mathrm{IX}} = -D_{\mathrm{H_2O\text{-}H_2}}\left(C_{\mathrm{IX}} - C_{\mathrm{VIII}}\right)/d_{\mathrm{Rib}}e_{\mathrm{Rib}} \tag{23}$$

$$w_{\mathrm{X}} = -D_{\mathrm{H_2O\text{-}H_2}}\left(C_{\mathrm{X}} - C_{\mathrm{IX}}\right)/d_{\mathrm{sep}}e_{\mathrm{sep}} = -D_{\mathrm{H_2O\text{-}H_2}}\left(C_{\mathrm{IV}} - C_{\mathrm{IX}}\right)/d_{\mathrm{sep}}e_{\mathrm{sep}} \tag{24}$$

$$w_{\mathrm{cathode}} = \left(C_{\mathrm{cat}} - C_{\mathrm{IV}}\right)D_{\mathrm{H_2O\text{-}H_2}}\Big/\left(d_{\mathrm{GDL}}e_{\mathrm{GDL}} + d_{\mathrm{Rib}}e_{\mathrm{Rib}} + d_{\mathrm{sep}}e_{\mathrm{sep}} + d_{\mathrm{MPL}}e_{\mathrm{MPL}}\right) \tag{25}$$

$$\begin{aligned} w_{\mathrm{anode}} = \left(C_{\mathrm{cat}} - C_{\mathrm{IV}}\right)\Big/\Big\{&d_{\mathrm{PEM}}e_{\mathrm{PEM}}/D_{\mathrm{PEM}} + \left(d_{\mathrm{cat}}e_{\mathrm{cat}} + d_{\mathrm{GDL}}e_{\mathrm{GDL}}\right. \\ &\left. + d_{\mathrm{Rib}}e_{\mathrm{Rib}} + d_{\mathrm{sep}}e_{\mathrm{sep}} + d_{\mathrm{MPL}}e_{\mathrm{MPL}}\right)/D_{\mathrm{H_2O\text{-}O_2}}\Big\} \end{aligned} \tag{26}$$

where $D_{\mathrm{H_2O\text{-}O_2}}$ means the binary diffusivity of H_2O and O_2 (m^2/s), C_{I} means the H_2O vapor concentration on the interface between MPL and GDL at cathode (kg/m^3), C_{cat} means the H_2O vapor concentration in catalyst layer at cathode (kg/m^3), C_{II} means the H_2O vapor concentration on the interface between GDL and separator rib or separator channel at cathode (kg/m^3), C_{III} means the H_2O vapor concentration on the interface between separator rib or separator channel and separator except for rib at cathode (kg/m^3), C_{IV} means the H_2O vapor concentration on the surface of separator's back surface at cathode (=H_2O vapor concentration in the experimental room) (kg/m^3), D_{PEM} means diffusivity of H_2O vapor in PEM (m^2/s), C_{V} means the H_2O vapor concentration on the interface between PEM and catalyst layer at cathode (kg/m^3), $D_{\mathrm{H_2O\text{-}H_2}}$ means binary diffusivity of H_2O and H_2 (m^2/s), C_{VI} means the H_2O vapor concentration on the interface between catalyst layer and MPL at anode (kg/m^3), C_{VII} means the H_2O vapor concentration on the interface between MPL and GDL at anode (kg/m^3), C_{VIII} means the H_2O vapor concentration on the interface between GDL and separator rib or separator channel at anode (kg/m^3), C_{IX} means the H_2O vapor concentration on the interface between separator rib and separator channel at anode(kg/m^3), and C_{X} means the H_2O vapor concentration on the surface of separator's back surface at anode (=C_{IV}=H_2O vapor concentration in the air in the experimental room) (kg/m^3). This study changes C_{IV} by 20% RH, 40% RH, 60% RH and 80% RH in order to evaluate the effect on the distribution of T_{react}. In this calculation, the thermal conductivity of each gas is estimated by the above mentioned H_2O vapor transfer [36].

The temperatures are measured by means of the thermograph to be substituted into the formulas as $T_{\mathrm{surf,c}}$ and $T_{\mathrm{surf,a}}$ to solve Equations (6)-(9). **Table 3**

Table 3. Power generation operation conditions to measure temperature by means of thermograph.

Initial temperature of cell (T_{ini}) [˚C]	100	
Load current of cell (A) (current density [A/cm^2])	20 (0.80)	
Condition of supply gas		
	Anode	Cathode
Gas type	H_2	O_2
Temperature of supply gas at inlet [˚C]	100	100
Relative humidity (RH) of supply gas [% RH]	40, 80	40, 80
Pressure of supply gas at inlet (absolute) [MPa]	0.4	0.4
Flow rate of supply gas at inlet [NL/min] (stoichiometric ratio [-])	0.210 (1.5), 0.280 (2.0), 0.420 (3.0)	0.105 (1.5), 0.140 (2.0), 0.210 (3.0)

shows the operation conditions which are used for the power generation experiment in order to measure the temperatures by means of thermograph. The data obtained under these experimental conditions have been used for 1D multi-plate heat transfer analysis. This study keeps the current density at 0.80 A/cm^2 in the power generation experiment in order to obtain the temperature data by means of thermograph. This study obtains the temperature distribution data caused by the reaction heat at the separator back. The author's previous studies have already explained the experimental procedure to measure the temperature during power generation [28] [29].

The authors show **Figure 3** to explain the segment division procedure using the example data of temperature image measured by thermograph. **Figure 3** does not show the specific experimental data. It is seen from **Figure 3** that we divide the in-plane temperature distribution into the segment with size of 10 mm × 10 mm each in order to apply the temperature data measured by means of thermograph for the heat transfer model proposed by this study. Although the power generation area is 50 mm × 50 mm, this study sets the observation area at the size of 40 mm × 50 mm in order to avoid leaking a gas via observation window in the experiments. The both gas channel width and rib width of separator are 1.0 mm and the number of gas channel is 5. Each segment is composed of five parts of rib and gas channel. This study considers the mean temperature in each segment at anode and cathode for the separator's back temperature in the proposed heat transfer model. **Figure 3** shows the segments named from A to T along with the gas flow direction.

It can be seen in **Figure 3** the insulators which cover the gas pipes disrupt the thermograph measurement regarding the area of segments A and T. We obtain the effective temperatures of segments A and T by eliminating the temperature data interrupted by the insulator from the all temperature data in each segment. This study assumes that $T_{surf,c}$ on the rib side equals to $T_{surf,c}$ on the channel sides

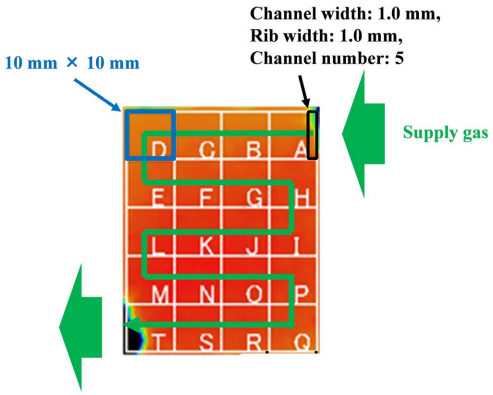

Figure 3. Segment division procedure of in-plane temperature distribution image measured by means of thermograph.

as well as $T_{\text{surf,a}}$ because we cannot recognize the difference between them by means of the measured data [28] [29].

According to the above mentioned assumptions and Equations (6) - (14), the reaction surface temperature T_{react} can be obtained as follows:

$$\begin{aligned} T_{\text{react}} = T_{\text{react,rib}} = T_{\text{react,chan}} = \left\{2H_{\text{react}}/A + \left(K_{\text{rib,c}} + K_{\text{chan,c}}\right)T_{\text{surf,c}}\right. \\ \left. + \left(K_{\text{rib,a}} + K_{\text{chan,a}}\right)T_{\text{surf,a}}\right\} \Big/ \left(K_{\text{rib,c}} + K_{\text{chan,a}} + K_{\text{rib,a}} + K_{\text{chan,a}}\right) \end{aligned} \quad (27)$$

where T_{react} can be estimated by H_{react} without calculating the local heat flux for each segment. Here, H_{react} is applied to estimate T_{react}, which is used as a constant irrespective of the segment. In addition, i indicates the segment.

2.4. Validation

Compared with the other reported heat transfer models [35] [40] [41] considering heat transfer conditions, the model developed by the authors [24] [25] [26] [27] [32] [42] has some difference. However, we have confirmed the temperature gradients for the targeted regions are almost the same tendency under the similar operational conditions [42]. In addition, the authors [43] have already simulated by the commercial CFD software with 3D model in order to predict the distributions of T_{react}. This 3D model bases on the governing equations consisting of conservation equations of mass, momentum, energy in porous region and electro-chemical reaction. According to the comparison of the results of numerical simulation using 3D model with that of 1D model developed by this study under the various operation conditions, the differences of T_{react} between two different models were from approximately 0.1˚C to 1.5˚C. Therefore, the 1D model developed by the authors could be validated by the 3D model. Consequently, we can consider that the heat transfer model developed by this study is reasonable. In addition, the authors think 1D model can save the research time and provide to understand the phenomena and mechanism in single cell of PEFC easily compared to 3D model if the accuracy of 1D model is confirmed. The authors also think that the simple analysis using 1D model is meaningful to speed up the R & D on PEFC.

3. Results

3.1. Effect of Flow Rate of Supply Gas and RH of Air Surrounding Cell of PEFC on Distribution of T_{react}-T_{ini}

It is necessary to clarify the effect of flow rates of supply gases on heat and mass transfer phenomena and power generation characteristics for managing the operation conditions. Figure 4 exhibits the effect of stoichiometric ratio (s.r.) of supply gases on distribution of T_{react}-T_{ini} calculated by the heat transfer model proposed by this study. As to the RH of supply gases at the inlet, it is 80% RH at anode and 80% RH at cathode (*i.e.*, A 80% RH, C 80% RH), respectively. Regarding the s.r. of supply gas at the inlet, it is set at 1.5, 2.0 and 3.0. The separator thickness is 2.0 mm.

It is seen from Figure 4 that the effect of flow rate of supply gases on distribution of T_{react}-T_{ini} is not large. Gas supply for power generation at s.r. = 1.5 [24] [26] is sufficient for power generation. In addition, it is confirmed the effect of flow rate of supply gases on distributions of T_{react}-T_{ini} is not significant regardless of RH condition, T_{react}-T_{ini} and separator thickness investigated in this study. The power output is nearly the same among various s.r. according to the power generation experiments in this study [28] [29]. In the following section, the results obtained with s.r. = 1.5 are analyzed as the representative case.

Additionally, it is important to understand the effect of RH of air surrounding single PEFC on distribution of T_{react}-T_{ini} which is estimated by the heat transfer model proposed by this study. Figure 5 shows the effect of RH of air surrounding single PEFC on distribution of T_{react}-T_{ini}. The RH of supply gases is A 80% RH, C 80% RH. As to the s.r. of supply gas, it is 1.5. The separator thickness is 2.0 mm. The RH of air surrounding single PEFC is changed from 20% RH to 80% RH.

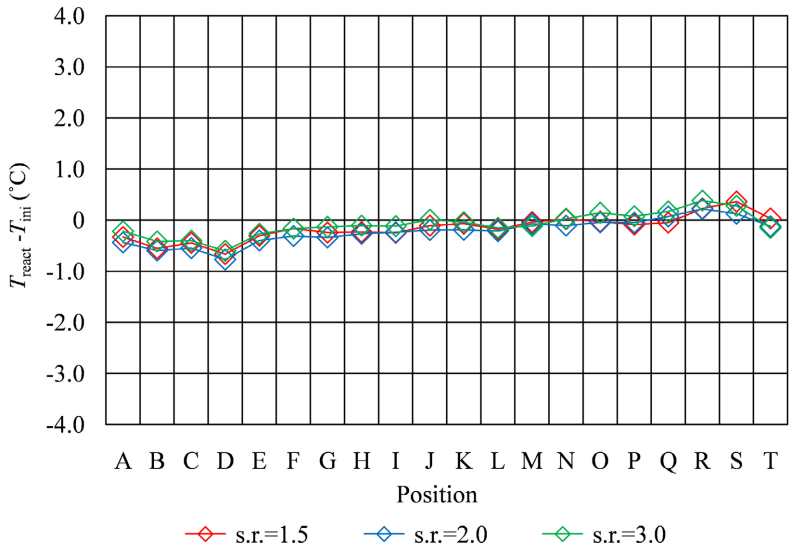

Figure 4. Effect of stoichiometric ratio on distribution of T_{react}-T_{ini} (A 80% RH, C 80% RH; relative humidity = 60% RH; separator thickness = 2.0 mm).

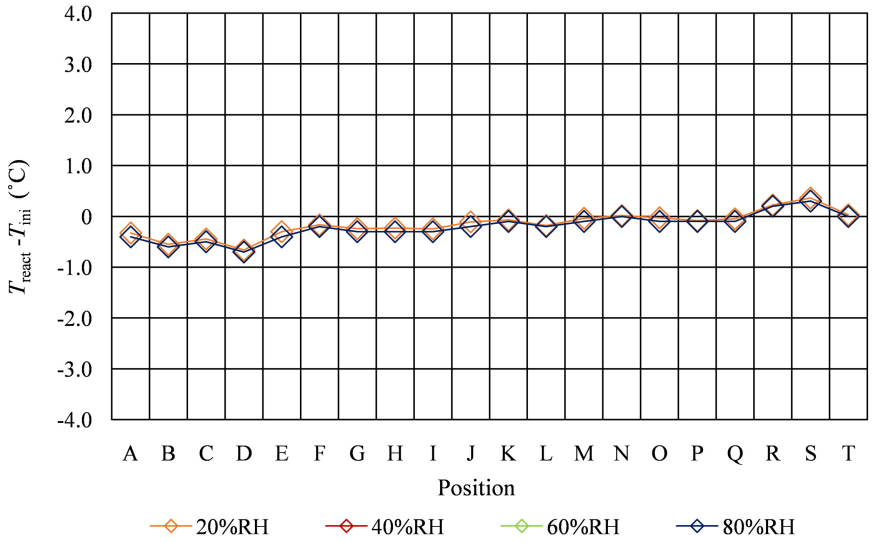

Figure 5. Effect of RH of air surrounding single PEFC on distribution of T_{react}-T_{ini} (A 80% RH, C 80% RH; s.r. = 1.5; separator thickness = 2.0 mm).

It is obvious from **Figure 5** that the effect of RH of air surrounding single PEFC on distribution of T_{react}-T_{ini} is small. It can be also confirmed under the other conditions investigated in this study. The digit of C_{cat} is 2 to 4 times as large as that of C_{IV}. We can think that the effect of RH of air surrounding single PEFC, *i.e.*, C_{IV} on distribution of T_{react}-T_{ini} is smaller. The annual mean RH of atmospheric air in Tsu City, Mie Prefecture, Japan in 2021 where the authors live is 63% RH [44]. In the following section, the results gotten by assuming C_{IV} of 60% RH are displayed.

3.2. Effect of Separator Size with RH on Distribution of T_{react}-T_{ini}

Figures 6-9 show comparison of distribution of T_{react}-T_{ini} among different separator thicknesses and RHs, respectively. The separator thickness is changed by 2.0 mm (saddle thickness = 1.0 mm, channel height = 1.0 mm), 1.5 mm (saddle thickness = 0.5 mm, channel height = 1.0 mm) and 1.0 mm (saddle height = 0.5 mm, channel height = 0.5 mm). RH is changed by A 80% RH, C 80% RH, 80% & RH at anode and 40% RH at cathode (A 80% RH, C 40% RH), 40% RH at anode and 80% RH at cathode (A 40% RH, C 80% RH) and 40% RH at anode and 40% RH at cathode (A 40% RH, C 40% RH). In addition, **Figures 10-13** show comparison of polarization curves among different thicknesses and RHs, respectively. The polarization curves were obtained from the power generation experiment.

According to **Figures 6-9**, we can observe that the temperature declines at the position D, L and T in case of separator thickness of 2.0 mm irrespective of RH, resulting in wider temperature distribution. In addition, the temperature in case of separator thickness of 2.0 mm is lower than that in case of separator thickness of 1.5 mm and 1.0 mm. In the experiment to obtain $T_{sur,a}$ and $T_{surf,c}$ by thermograph, the temperature is measured after confirming the steady state [29]. Since

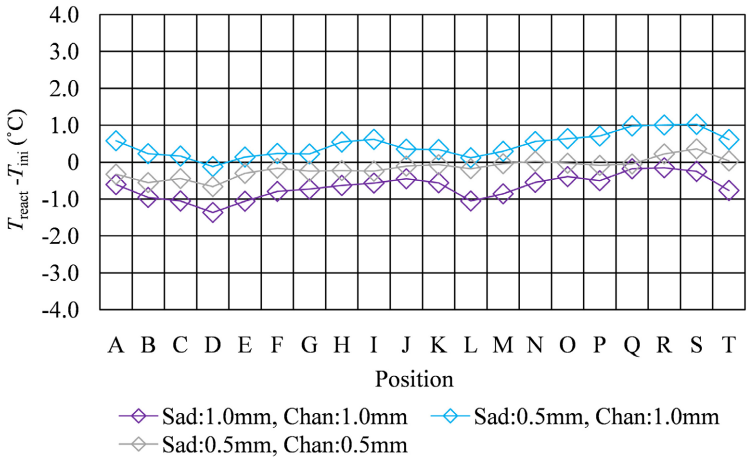

Figure 6. Effect of separator thickness on distribution of T_{react}-T_{ini} (A 80% RH, C 80% RH).

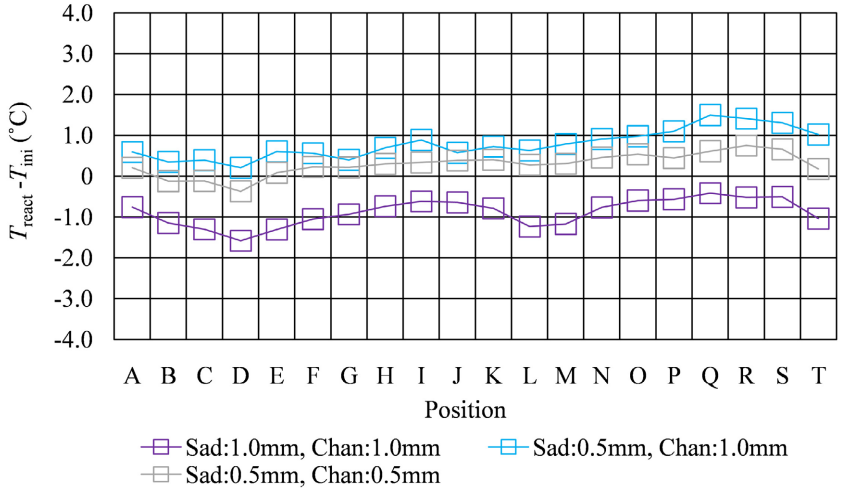

Figure 7. Effect of separator thickness on distribution of T_{react}-T_{ini} (A 80% RH, C 40% RH).

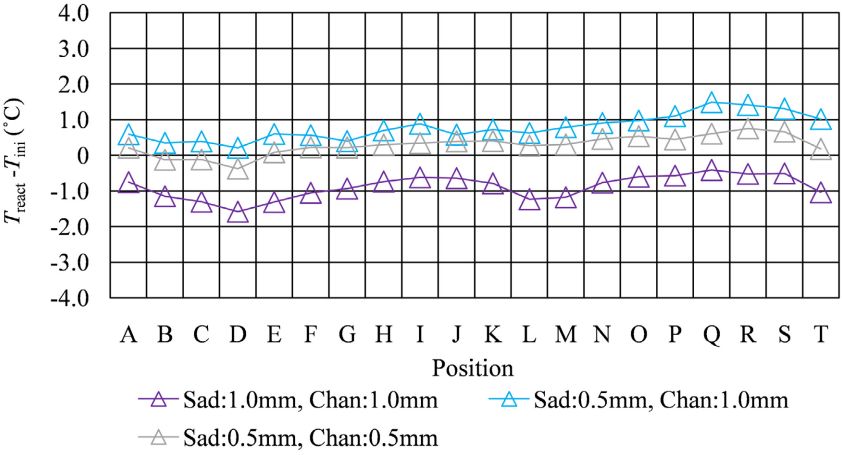

Figure 8. Effect of separator thickness on distribution of T_{react}-T_{ini} (A 40% RH, C 80% RH).

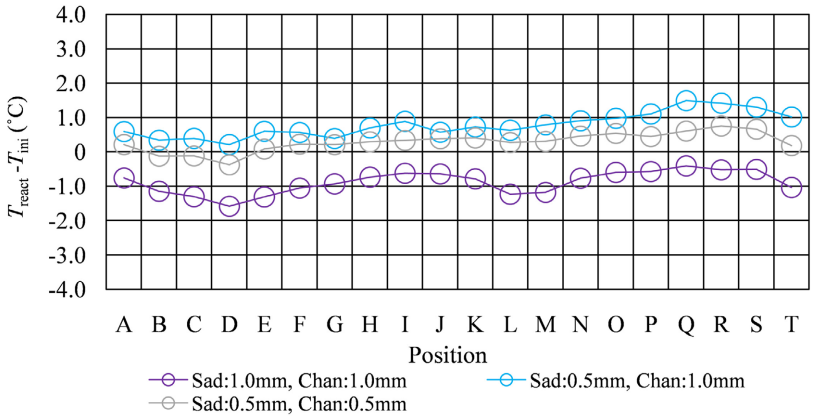

Figure 9. Effect of separator thickness on distribution of T_{react}-T_{ini} (A 40% RH, C 40% RH).

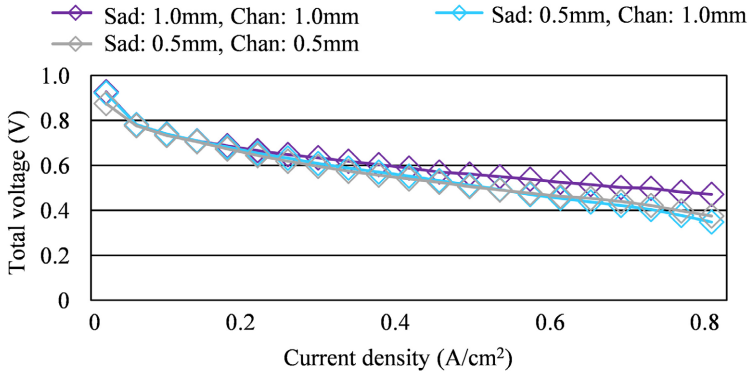

Figure 10. Comparison of polarization curves among various separator thicknesses (A 80% RH, C 80% RH).

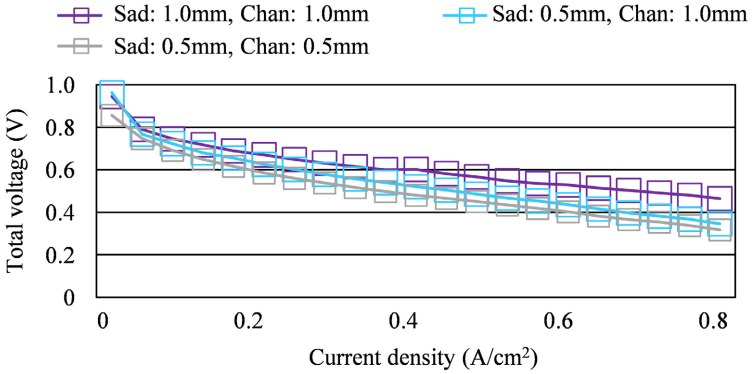

Figure 11. Comparison of polarization curves among various separator thicknesses (A 80% RH, C 40% RH).

the heat capacity of separator thickness of 2.0 mm is larger, it is thought that the whole cell temperature after balancing with the atmospheric air is lower compared to the other considered separator thicknesses [45]. If the whole cell temperature decreases, the actual RH increases. This is due to exponential increasing saturation of H_2O vapor with temperature [46]. It is thought that the H_2O water

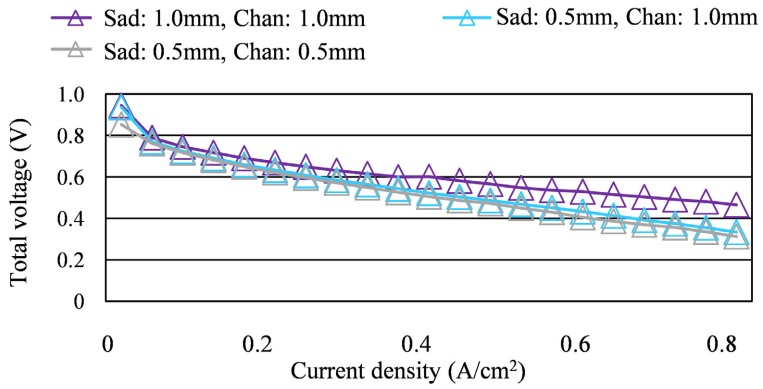

Figure 12. Comparison of polarization curves among various separator thicknesses (A 40% RH, C 80% RH).

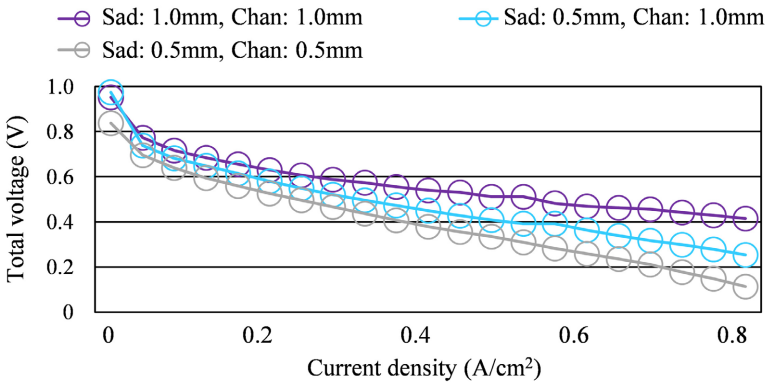

Figure 13. Comparison of polarization curves among various separator thicknesses (A 40% RH, C 40% RH).

concentration is higher at the position L which is positioned at the corner of serpentine separator. As a result, the gas diffusion in GDL and catalyst layer might be disrupted, which causes the decrease in the kinetics of electro-chemical reaction. Consequently, the temperature declines at the position L since the power generation performance is declined. As to the position T, it is thought that the H_2O water concentration is higher because the H_2O with gas flow concentrates at the outlet of the cell [24] [25] and well hydration. Therefore, the temperature declines at the position L and T are remarkable in case of separator thickness of 2.0 mm compared to the other separator cases. Regarding the position D, it is the inlet of the anode side. Therefore, the cell is cooled by the gas since the supplied gas is colder than the single PEFC heated by reaction heat [24] [46].

According to **Figures 6-9**, we can observe the temperature increases along with the gas flow through the gas channel by approximately 1˚C in case of separator thickness of 1.5 mm and 1.0 mm. The PEM is hydrated by not only the H_2O produced by electro-chemical reaction but also the humidified gas flows through the gas channel, indicating the power generation is progressed along with the gas flow [25] [26].

We can see from Figures 10-13 that the power generation performance declines with the reduction in separator thickness especially at high current density such as 0.80 A/cm^2 and low RH condition, *i.e.* A 40% RH, C 40% RH. The heat capacity is smaller with the decrease in separator thickness, resulting that the cell of PEFC is easy to be dehydrated [45]. Under the high current density condition which produces larger heat by reaction as well as dry condition, the cell of PEFC is dehydrated more. Therefore, the power generation performance declines.

3.3. Evaluation on Standard Deviation of Distribution of T_{react}

Figures 14-16 display the relation between standard deviation of distribution of T_{react}-T_{ini} and total voltage obtained in the experiment changing the separator thickness. The data under different s.r. and RH conditions are shown in each figure. The approximate line is also shown in each figure.

It is seen from Figures 14-16 that the slope of approximate line for the relation between standard deviation of distribution of T_{react}-T_{ini} and total voltage is negative. It can be claimed that the wider temperature distribution provides the

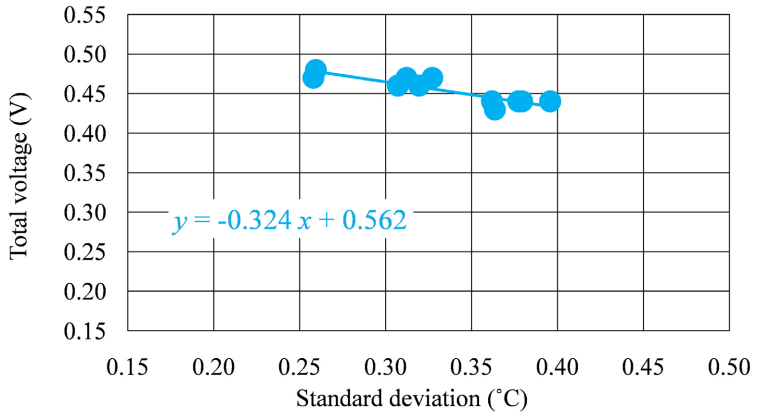

Figure 14. Relation between standard deviation of distribution of T_{react}-T_{ini} and total voltage (separator thickness = 2.0 mm).

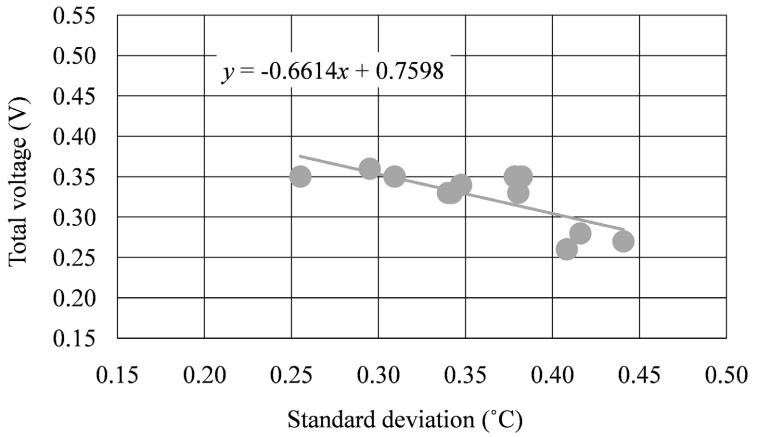

Figure 15. Relation between standard deviation of distribution of T_{react}-T_{ini} and total voltage (separator thickness = 1.5 mm).

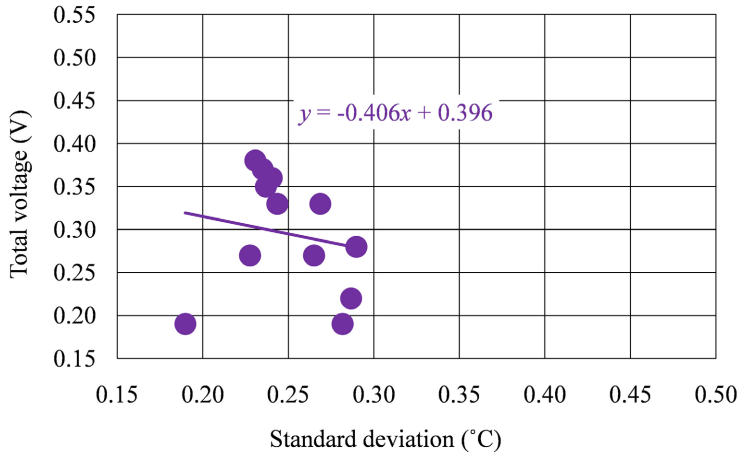

Figure 16. Relation between standard deviation of distribution of T_{react}-T_{ini} and total voltage (separator thickness = 1.0 mm).

reduction in power generation performance. In addition, we can see from **Figures 14-16** that the total voltage drops with the reduction in separator thickness. The total voltage drops at the high current density such as 0.80 A/cm^2, which was set in the power generation experiment in order to measure $T_{surf,a}$ and $T_{surf,c}$ by thermograph, is larger with the decrease in separator thickness [45] since the drying impact is larger. Therefore, the total voltage decreases with the decrease in separator thickness. Moreover, as to the case of separator thickness of 1.0 mm, it is found that the distribution range of standard deviation of T_{react}-T_{ini} is smaller compared to the other separator cases, while the total voltage shows the larger variation compared to the other separator cases. The separator thickness of 1.0 mm consists of saddle thickness of 0.5 mm and channel height of 0.5 mm. Since the channel cross sectional area is a half compared to the other separator cases, the velocity and concentration of gas is larger, resulting that the fuel and oxidant can be supplied to the catalyst layer well. Therefore, it seems that the distribution of T_{react}-T_{ini} becomes more even, which indicates the distribution range of standard deviation of T_{react}-T_{ini} is smaller. On the other hand, it is thought PEM and catalyst layer are dehydrated easily in case of separator thickness of 1.0 mm due to smaller heat capacity [45]. Especially, the power generation performance declines in case of separator thickness of 1.0 mm under low RH condition due to dehydration caused by small heat capacity [45]. Therefore, the power generation performance is influenced by RH condition and temperature distribution strictly. Regarding **Figure 16**, the data with small standard deviation of 0.19˚C and small total voltage of 0.19 V are obtained under the low RH condition such as A 40% RH, C 40% RH. This type of low RH condition causes the other data exhibiting low total voltage shown in **Figure 16**. Consequently, it is believed that the power generation performance in case of separator thickness of 1.0 mm is influenced by the decrease in cross sectional area as well as dehydration, resulting that the total voltage shows the larger variation compared to the other separator cases.

Summarizing the results and discussion, we can suggest that thin separators (such as the thickness of 1.5 mm and 1.0 mm) are not suitable for higher temperature operation than usual. This study thinks a smaller distribution range of the standard deviation of T_{react}-T_{ini} is obtained in the case of separator thickness of 1.0 mm because of low power generation performance. Since the heat capacity of thinner separator is smaller, the cell of PEFC is easy to be dehydrated due to the temperature rise. H^+ conductivity of PEM and the activity of catalyst are lower under dry conditions, resulting that the power generation performance declines. In addition, the electrochemical reaction is not progressed well under dry conditions, resulting that H_2O and reaction heat are not produced well. It is thought that the produced H_2O and generated reaction heat cause the wider in-plane temperature distribution. From the polarization curves, as shown before, the power generation performance decreases with the reduction in the separator thickness, especially at the current density of 0.80 A/cm^2 where the in-plane distribution of T_{surf} was measured by means of thermograph in the experiment. We can say that the lower power generation performance condition is not suitable for application at T_{ini} = 100˚C. Therefore, this study claims that the thinner separators are not suitable for application at high temperatures such as T_{ini} = 100˚C. Since the control of humidification, as well as in-plane distribution of T_{react}-T_{ini} at a higher temperature, is stricter than usual operation temperature, hydration of supply gas and thermal properties of cell components of PEFC should be considered for analyzing electrochemical reaction. According to the state-of-art review on research and development of separators [47] [48] [49], the material type composite and surface coating processes have been investigated to improve the conductivity and H_2O behavior. However, the thermal properties of the separator have not been investigated yet. Therefore, this study would like to suggest that the thermal properties of the separator such as heat capacity and thermal conductivity should be improved to obtain better power generation performance.

4. Conclusions

This study has examined the effect of separator thickness on the distribution of T_{react}-T_{ini} in single PEFC changing flow rates and RHs of supply gases at T_{ini} = 100˚C. The distribution of T_{react} has been evaluated by the heat transfer model considering H_2O vapor transfer, which uses the separator's back temperature measured by thermograph experimentally. The following conclusions are obtained from this study:

1) The effect of the flow rate of supply gases on the distribution of T_{react}-T_{ini} is not large among the investigated conditions.

2) The effect of RH of air surrounding a single PEFC on the distribution of T_{react}-T_{ini} is not significant among the investigated conditions.

3) The temperature declines at positions D, L and T in case of separator thickness of 2.0 mm through the temperature increases along with the gas flow with the gas channel by approximately 1˚C in case of separator thickness of 1.5 mm

and 1.0 mm.

4) It is revealed that the slope of the approximate line for the relation between the standard deviation of the distribution of T_{react}-T_{ini} and total voltage is negative, indicating that the wider temperature distribution provides the reduction in power generation performance.

5) Regarding the case of separator thickness of 1.0 mm, it is revealed that the distribution range of standard deviation of T_{react}-T_{ini} is smaller compared to the other separator cases, while the total voltage shows a larger variation compared to the other separator cases.

6) This study claims that the thin separators, *i.e.* thickness of 1.5 mm and 1.0 mm are not suitable for higher temperature operation than usual.

7) In future work, this study suggests that the thermal properties of separators such as heat capacity and thermal conductivity should be improved to obtain a better power generation performance at higher temperature operation than usual.

Data Availability

The datasets generated and analyzed during this study are available from the corresponding author on reasonable request.

Conflicts of Interest

The authors state there is no conflict of interest.

References

[1] NEDO (New Energy and Industry Technology Development Organization) (2022). https://www.nedo.go.jp/cotent/100871973.pdf

[2] Zhang, G. and Kandlikar, S.G.A. (2012) Critical Review of Cooling Technique in Proton Exchange Membrane Fuel Cell Stacks. *International Journal of Hydrogen Energy*, **37**, 2412-2429. https://doi.org/10.1016/j.ijhydene.2011.11.010

[3] Mohamed, W.A.N.W., Talib, S.F.A., Zakaria, I.A., Mamat, A.M.I. and Daud, W.R.W. (2018) Effect of Dynamic Load on the Temperature Profiles and Cooling Response Time of a Proton Exchange Membrane Fuel Cell. *Journal of the Energy Institute*, **91**, 349-357. https://doi.org/10.1016/j.joei.2017.02.006

[4] Zhang, J., Zhang, C., Hao, D., Ni, M., Huang, S., Liu, D. and Zheng, Y. (2021) 3D Non-Isothermal Dynamic Simulation of High Temperature Proton Exchange Membrane Fuel Cell in the Start-Up Process. *International Journal of Hydrogen Energy*, **46**, 2577-2593. https://doi.org/10.1016/j.ijhydene.2020.10.116

[5] Lee, C.Y., Wang, F., Kuo, Y.W., Tsai, C.H., Cheng, Y.T., Cheng, C.K. and Lin, J.T. (2016) *In-Situ* Measurement of High-Temperature Proton Exchange Membrane Fuel Cell Stack Using Flexible Five-in-One Micro Sensor. *Sensors*, **16**, Article 1731. https://doi.org/10.3390/s16101731

[6] Zhang, J., Xie, Z., Zhang, J., Tang, Y., Song, C., Navessin, T., Shi, Z., Song, D., Wang, H., Wilikinson, D.P., Liu, Z.S. and Holdcroft, S. (2006) High Temperature PEM Fuel Cells. *Journal of Power Sources*, **160**, 872-891. https://doi.org/10.1016/j.jpowsour.2006.05.034

[7] Jin, C., Wang, T., Che, X., Dong, J., Liu, R. and Yang, J. (2022) New High-Performance Bulky N-Heterocyclic Group Functionalized Poly(Terphenyl Piperidinium) Mem-

branes for HT-PEMFC Applications. *Journal of Membrane Science*, **641**, Article ID: 119884. https://doi.org/10.1016/j.memsci.2021.119884

[8] Budak, Y. and Devrim, Y. (2022) Micro-Cogeneration Application for a High-Temperature PEM Fuel Cell Stack Operated with Polybenzimidazole Based Membranes. *International Journal of Hydrogen Energy*, **45**, 35198-35207. https://doi.org/10.1016/j.ijhydene.2019.11.173

[9] Ryu, S.K., Vinothkannan, M., Kim, A.R. and Yoo, D.J. (2022) Effect of Type and Stoichiometry of Fuels on Performance of Polybenzimidazole-Based Proton Exchange Membrane Fuel Cells Operating at the Temperature Range of 120 - 160 ˚C. *Energy*, **238**, Article ID: 121791. https://doi.org/10.1016/j.energy.2021.121791

[10] Kim, D.H., Min, C.M., Lee, E., Lee, J.S. and Pak, C. (2020) Effect of Vinylphosphonic Acid and Polymer Binders with Phosphate Groups on Performance of High-Temperature Polymer Electrolyte Membrane Fuel Cell. *Catalysis Today*, **358**, 333-337. https://doi.org/10.1016/j.cattod.2019.07.046

[11] Jia, T., Shen, S., Zhao, J., Jin, J., Pan, B., Duan, X., Meng, C. and Che, Q. (2020) Ultrathin Membranes Formation via the Layer by Layer Self-Assembly of Carbon Nanotubes-Based Inorganics as High Temperature Proton Exchange Membranes. *International Journal of Hydrogen Energy*, **45**, 14517-14527. https://doi.org/10.1016/j.ijhydene.2020.03.175

[12] Wang, D., Wang, S., Tain, X., Li, J., Liu, F., Wang, X., Chen, H., Mao, T. and Liu, G. (2020) Ethyl Phosophoric Acid Grafted Amino-Modified Polybenzimidazole with Improved Long-Term Stability for High-Temperature Proton Exchange Membrane Proton Exchange Membrane Applications. *International Journal of Hydrogen Energy*, **45**, 3176-3185. https://doi.org/10.1016/j.ijhydene.2019.11.219

[13] Zhang, J., Wang, H., Li, W., Zhang, J., Lu, D., Yan, W., Xiang, Y. and Lu, S. (2021) Effect of Catalyst Layer Microstructures on Performance and Stability for High Temperature Polymer Electrolyte Membrane Fuel Cells. *Journal of Power Sources*, **505**, Article ID: 230059. https://doi.org/10.1016/j.jpowsour.2021.230059

[14] Lee, W.J., Lee, J.S., Park, H.Y., Park, H.S., Lee, S.Y., Song, K.H. and Kim, H. (2020) Improvement of Fuel Cell Performances through the Enhanced Dispersion of the PEFC Binder in Electrodes for Use in High Temperature Polymer Electrolyte Membrane Fuel Cells. *International Journal of Hydrogen Energy*, **45**, 32825-32833. https://doi.org/10.1016/j.ijhydene.2020.03.095

[15] Xu, Y., Fan, R., Chang, G., Xu, S. and Cai, T. (2021) Investigating Temperature-Driven Water Transport in Cathode Gas Diffusion Media of PEMFC with a Non-Isothermal, Two-Phase Model. *Energy Conversion and Management*, **248**, Article ID: 114791. https://doi.org/10.1016/j.enconman.2021.114791

[16] Xia, L., Ni, M., Xu, Q., Xu, H. and Zheng, K. (2021) Optimization of Catalyst Layer Thickness for Achieving High Performance and Low Cost of High Temperature Proton Exchange Membrane Fuel Cell. *Applied Energy*, **294**, Article ID: 117012. https://doi.org/10.1016/j.apenergy.2021.117012

[17] Das, S.K. and Gibson, H.A. (2021) Three Dimensional Multi-Physics Modeling and Simulation for Assessment of Mass Transport Impact on the Performance of a High Temperature Polymer Electrolyte Fuel Cell. *Journal of Power Sources*, **499**, Article ID: 229844. https://doi.org/10.1016/j.jpowsour.2021.229844

[18] Xia, L., Ni, M., He, Q., Xu, Q. and Cheng, C. (2021) Optimization of Gas Diffusion Layer in High Temperature PEMFC with the Focuses on Thickness and Porosity. *Applied Energy*, **300**, Article ID: 117357. https://doi.org/10.1016/j.apenergy.2021.117357

[19] Huang, T., Wang, W., Yuan, Y., Huang, J., Chen, W., Zhang, J., Kong, X., Zhang, Y. and Wan, Z. (2021) Optimization of High-Temperature Proton Exchange Membrane Fuel Cell Flow Channel Based on Genetic Algorithm. *Energy Reports*, **7**, 1374-1384. https://doi.org/10.1016/j.egyr.2021.02.062

[20] Chen, H., Guo, H., Ye, F. and Ma, C.F.A. (2021) Numerical Study of Oriented-Type Flow Channels with Porous-Blocked Baffles of Proton Exchange Membrane Fuel Cells. *International Journal of Hydrogen Energy*, **46**, 29443-29458. https://doi.org/10.1016/j.ijhydene.2020.12.178

[21] Zhang, T., Li, J., Li, Q., Yu, M. and Sun, H. (2021) Combination Effects of Flow Field Structure and Assembly Force on Performance of High Temperature Proton Exchange Membrane Fuel Cells. *International Journal of Energy Research*, **45**, 7903-7917. https://doi.org/10.1002/er.6374

[22] Xia, L., Xu, Q., He, Q., Ni, M. and Seng, M. (2021) Numerical Study of High Temperature Proton Exchange Membrane Fuel Cell (HT-PEMFC) with a Focus on Rib Design. *International Journal of Hydrogen Energy*, **46**, 21098-21111. https://doi.org/10.1016/j.ijhydene.2021.03.192

[23] Nanadegani, F.S., Lay, E.N. and Sunden, B. (2020) Computational Analysis of the Impact of a Micro Porous Layer (MPL) on the Characteristics of a High Temperature PEMFC. *Electrochimica Acta*, **333**, Article ID: 135552. https://doi.org/10.1016/j.electacta.2019.135552

[24] Nishimura, A., Kono, N., Toyoda, K., Kojima, M. and Kolhe, M.L. (2021) Impact Analysis of MPL on a PEFC Cell's Temperature Distribution with Thin PEM and GDL for Operating at Higher Temperature than Usual. *Journal of Energy and Power Engineering*, **15**, 39-51. https://doi.org/10.17265/1934-8975/2021.02.001

[25] Nishimura, A., Yamamoto, K., Okado, T., Kojima, Y., Hirota, M. and Kolhe, M. (2020) Impact of Analysis of MPL and PEM Thickness on Temperature Distribution within PEFC Operating at Relatively Higher Temperature. *Energy*, **205**, Article ID: 117875. https://doi.org/10.1016/j.energy.2020.117875

[26] Nishimura, A., Sato, Y., Kamiya, S., Okado, T., Yamamoto, K., Hirota, M. and Hu, E. (2019) Impact of Thickness of Polymer Electrolyte Membrane and Gas Diffusion Layer on Temperature Distribution in Polymer Electrolyte Fuel Cell Operated at Temperature around 90 ˚C. *Journal of Energy and Power Engineering*, **13**, 97-115. https://doi.org/10.17265/1934-8975/2019.03.002

[27] Nishimura, A., Sato, Y., Yoshimura, M., Kamiya, S. and Hirota, M. (2018) Impact of Thickness of Polymer Electrolyte Membrane on Temperature Distribution in Single Cell of Polymer Electrolyte Fuel Cell Operated at High Temperature. *Journal of Energy and Power Engineering*, **12**, 80-92. https://doi.org/10.17265/1934-8975/2018.02.004

[28] Nishimura, A., Shibuya, K., Morimoto, A., Tanaka, S., Hirota, M., Nakamura, Y., Kojima, M., Narita, M. and Hu, E. (2012) Dominant Factor and Mechanism of Coupling Phenomena in Single Cell of Polymer Electrolyte Fuel Cell. *Applied Energy*, **90**, 73-79. https://doi.org/10.1016/j.apenergy.2011.01.003

[29] Nishimura, A., Okado, T., Kojima, Y. and Hu, E. (2021) Impact of Microporous Layer on Heat and Mass Transfer in a Single Cell of Polymer Electrolyte Fuel Cell Using a Thin Polymer Electrolyte Membrane and a Thin Gas Diffusion Layer Operated at a High-Temperature Range. *ACS Omega*, **6**, 14575-14584. https://doi.org/10.1021/acsomega.1c01693

[30] Zamel, N., Becker, J. and Wiegmann, A. (2012) Estimating the Thermal Conductivity and Diffusion Coefficient of the Microporous Layer of Polymer Electrolyte Membrane

Fuel Cells. *Journal of Power Sources*, **207**, 70-80.
https://doi.org/10.1016/j.jpowsour.2012.02.003

[31] Chen, G., Zhang, G., Guo, L. and Liu, H. (2016) Systematic Study on the Functions and Mechanisms of Micro Porous Layer on Water Transport in Proton Exchange Membrane Fuel Cells. *International Journal of Hydrogen Energy*, **41**, 2334-2441.
https://doi.org/10.1016/j.ijhydene.2016.01.074

[32] Nishimura, A., Fukuoka, T., baba, M., Hirota, M. and Hu, E. (2015) Clarification of Temperature Distribution in Single Cell of Polymer Electrolyte Fuel Cell under Different Operation Conditions by Means of 1D Multi-Plate Heat-Transfer Model. *Journal of Chemical Engineering of Japan*, **48**, 862-871.
https://doi.org/10.1252/jcej.14we200

[33] Alizadeh, E., Rahmi-Ebso, M., Rahgoshay, S.M. and Saadat, S.H.M. (2017) Numerical and Experimental Investigation of Cascade Type Serpentine Flow Filed of Reactant Gases for Improving Performance of PEM Fuel Cell. *International Journal of Hydrogen Energy*, **42**, 14708-14724. https://doi.org/10.1016/j.ijhydene.2017.04.212

[34] Copper, N.J., Santamaria, A.D., Becton, M.K. and Park, J.W. (2017) Neutron Radiography Measurements of *In-Situ* PEMFC Liquid Water Saturation in 2D & 3D Morphology Gas Diffusion Layers. *International Journal of Hydrogen Energy*, **42**, 14708-14724. https://doi.org/10.1016/j.ijhydene.2017.05.105

[35] Khandewal, M. and Mench, M.M. (2006) Direct Measurement of Though-Plane Thermal Conductivity and Contract Resistance in Fuel Cell Materials. *Journal of Power Sources*, **161**, 1106-1115. https://doi.org/10.1016/j.jpowsour.2006.06.092

[36] The Japan Society of Mechanical Engineers (1993) JSME Heat Transfer Handbook. Maruzen, Tokyo, 367-369.

[37] Nishimura, A., Toyoda, K., Kojima, Y., Ito, S. and Hu, E. (2021) Numerical Simulation on Impacts of Thickness of Nafion Series Membranes and Relative Humidity on PEMFC Operated at 363 K and 373 K. *Energies*, **14**, Article 8256.
https://doi.org/10.3390/en14248256

[38] Sunakawa, D., Oyama, S., Araki, T. and Onda, K. (2006) Measurement of Diffusion Coefficient and Electro-Osmotic Coefficient of Water at PEFC. *Electrochemistry*, **74**, 732-736. https://doi.org/10.5796/electrochemistry.74.732

[39] Reid, R.C., Prausnitz, J.M. and Poling, B.E. (1987) The Properties of Gases and Liquids. McGraw-Hill Book Company, New York, 589-591.

[40] Kawase, M., Inagaki, T., Kawashimra, S. and Miura, K. (2009) Effective Thermal Conductivity of Gas Diffusion Layer in Through-Plane Direction. *ECS Transactions*, **25**, 1529-1537. https://doi.org/10.1149/1.3210709

[41] Jung, C.Y., Shim, H.S., Koo, S.M., Lee, S.H. and Yi, S.C. (2012) Investigation of the Temperature Distribution in Proton Exchange Membrane Fuel Cell. *Applied Energy*, **93**, 733-741. https://doi.org/10.1016/j.apenergy.2011.08.035

[42] Nishimura, A., Iio, K., Baba, M., Yamauchi, T., Hirota, M. and Hu, E. (2014) Modeling of Heat Transfer in Single Cell of Polymer Electrolyte Fuel Cell by Means of Temperature Data Measured by Thermograph. *Journal of Chemical Engineering of Japan*, **47**, 521-529. https://doi.org/10.1252/jcej.13we275

[43] Nishimura, A., Zamami, K. P., Yoshimura, M., Hirota, M. and Kolhe, M.L. (2017) Numerical Analysis of Temperature Distributions in Single Cell of Polymer Electrolyte Fuel Cell When Operated in Elevated Temperature Range. *Journal of Energy and Power Engineering*, **11**, 393-408.
https://doi.org/10.17265/1934-8975/2017.06.005

[44] Japan Meteorological Agency (2022) Weather Forecast.

[45] Nishimura, A., Kojima, Y., Ito, S. and Hu, E. (2022) Impacts of Separator Thickness on Temperature Distribution and Power Generation Characteristics of a Single PEMFC Operated at Higher Temperature of 363 and 373 K. *Energies*, **15**, Article 1558. https://doi.org/10.3390/en15041558

[46] Nishimura, A., Osada, K., Tsunoda, T., Yoshimura, M., Hirota, M. and Hu, E. (2016) Analysis on Temperature Distribution in Single Cell of Polymer Electrolyte Fuel Cell When Operated in High Temperature Range. *Journal of Energy and Power Engineering*, **10**, 453-464. https://doi.org/10.17265/1934-8975/2016.08.001

[47] Xu, Z., Qiu, D., Yi, P., Peng, L. and Lai, X. (2020) Towards Mass Applications: A Review on the Challenges and Developments in Metallic Bipolar Plates for PEMFC. *Progress in Natural Science*: *Materials International*, **46**, 8672-8701.

[48] Wu, S., Yang, W., Yan, H., Zuo, X., Cao, Z., Li, H., Shi, M. and Chen, H. (2021) A Review of Modified Metal Bipolar Plates for Proton Exchange Membrane Fuel Cells. *International Journal of Hydrogen Energy*, **46**, 8672-8701. https://doi.org/10.1016/j.ijhydene.2020.12.074

[49] Saadat, N., Dhakal, H.N., Tjong, J., Jaffer, S., Yang, W. and Sain, M. (2021) Recent Advances and Future Perspectives of Carbon Materials for Fuel Cell. *Renew and Sust. Energy Reviews*, **138**, Article ID: 110535. https://doi.org/10.1016/j.rser.2020.110535

Nomenclature

A: heat transfer area which equals to the active area of MEA [m^2]

C_{cat}: H_2O vapor concentration in catalyst layer at cathode side [kg/m^3]

C_I: H_2O vapor concentration on the interface between MPL and GDL at cathode side [kg/m^3]

C_{II}: H_2O vapor concentration on the interface between GDL and separator channel at cathode side [kg/m^3]

C_{III}: H_2O vapor concentration on the interface between separator rib or separator channel and separator except for rib at cathode side [kg/m^3]

C_{IV}: H_2O vapor concentration on the surface of separator's back surface at cathode side (=H_2O vapor concentration in the air in the experimental room) [kg/m^3]

C_V: H_2O vapor concentration on the interface between PEM and catalyst layer at cathode side [kg/m^3]

C_{VI}: H_2O vapor concentration on the interface between catalyst layer and MPL at anode side [kg/m^3]

C_{VII}: H_2O vapor concentration on the interface between MPL and GDL at anode side [kg/m^3]

C_{VIII}: H_2O vapor concentration on the interface between GDL and separator rib or separator channel at anode side [kg/m^3]

C_{IX}: H_2O vapor concentration on the interface between separator rib and separator channel at anode side [kg/m^3]

C_X: H_2O vapor concentration on the surface of separator's back surface at anode side [kg/m^3]

$D_{H_2O\text{-}H_2}$: binary diffusivity of H_2O and H_2 [m^2/s]

$D_{H_2O\text{-}O_2}$: binary diffusivity of H_2O and O_2 [m^2/s]

E_i: ideal energy generation rate from the H_2O formation by H_2 and O_2 estimated by higher heating value [W]

F: Faraday constant (=96,500) [C/mol]

$H_{chan,a}$: heat flux through channel of separator at anode side [W]

$H_{chan,c}$: heat flux through channel of separator at cathode side [W]

H_{react}: heat generation rate [W]

$H_{rib,a}$: heat flux through rib at anode side [W]

$H_{rib,c}$: heat flux through rib at cathode side [W]

I: load current [A]

i: segment [-]

$K_{chan,a}$: overall heat transfer coefficient through channel of separator at anode side [W/(m·K)]

$K_{chan,c}$: overall heat transfer coefficient through channel of separator at cathode side [W/(m·K)]

$K_{rib,a}$: overall heat transfer coefficient through rib at anode side [W/(m·K)]

$K_{rib,c}$: overall heat transfer coefficient through rib at cathode side [W/(m·K)]

k_{cat}: thermal conductivity of catalyst layer [W/(m·K)]

$k_{chan,a}$: thermal conductivity of mixed gas in channel of separator at anode side [W/(m·K)]

$k_{chan,c}$: thermal conductivity of mixed gas in channel of separator at cathode side [W/(m·K)]

k_{GDL}: thermal conductivity of GDL [W/(m·K)]

k_{MPL}: thermal conductivity of MPL [W/(m·K)]

k_{PEM}: thermal conductivity of PEM [W/(m·K)]

$k_{rib,a}$: thermal conductivity of separator rib at anode side [W/(m·K)]

$k_{rib,c}$: thermal conductivity of separator rib at cathode side [W/(m·K)]

k_{sep}: thermal conductivity of separator except for rib [W/(m·K)]

m_{H_2} : molar consumption rate of supplied H_2 [mol/s]

m_{O_2} : molar consumption rate of supplied O_2 [mol/s]

n: valence ion (=2) [-]

q_{HHV}: ideal energy generation rate estimated on higher heating value [kJ/mol]

s.r.: stoichiometric ratio [-]

T_{ini}: initial operation temperature [K or ˚C]

T_{react}: temperature of reaction surface [K or ˚C]

$T_{react,chan}$: temperature of reaction surface under separator channel [K or ˚C]

$T_{react,rib}$: temperature of reaction surface under separator rib [K or ˚C]

$T_{surf,a}$: separator's back surface temperature at anode side [K or ˚C]

$T_{surf,c}$: separator's back surface temperature at cathode side [K or ˚C]

V: total voltage obtained by the power generation experiment [V]

W_F: electric power generation by PEFC [W]

d_{cat}: thickness of catalyst layer [m]

d_{chan}: thickness of separator channel [m]

d_{GDL}: thickness of GDL [m]

d_{MPL}: thickness of MPL [m]

d_{PEM}: thickness of PEM [m]

d_{sep}: thickness of separator except for rib [m]